Nanoscale Res Lett (2007) 2:185–201
DOI 10.1007/s11671-007-9057-5

NANO REVIEW

Stretching and immobilization of DNA for studies of protein–DNA interactions at the single-molecule level

Ji Hoon Kim · Venkat Ram Dukkipati · Stella W. Pang · Ronald G. Larson

Received: 13 March 2007 / Accepted: 30 March 2007 / Published online: 18 April 2007

Abstract Single-molecule studies of the interactions of DNA and proteins are important in a variety of biological or biotechnology processes ranging from the protein's search for its DNA target site, DNA replication, transcription, or repair, and genome sequencing. A critical requirement for single-molecule studies is the stretching and immobilization of otherwise randomly coiled DNA molecules. Several methods for doing so have been developed over the last two decades, including the use of forces derived from light, magnetic and electric fields, and hydrodynamic flow. Here we review the immobilization and stretching mechanisms for several of these techniques along with examples of single-molecule DNA–protein interaction assays that can be performed with each of them.

Keywords DNA · Single-molecule · Proteins · DNA–protein interactions

Introduction

DNA is a semi-flexible polymer composed of deoxyribonucleotide triphosphates (dNTPs) that are joined together by phosphodiester bonds. Common examples include bacteriophage DNA molecules, such as λ and T7, which have been extensively used as templates for studying DNA–protein interactions [1–4]. The radius of gyration (R_g) of a self-avoiding polymer, such as a coiled DNA, quantifies its physical size in solution, and can be expressed as $\langle R_g^2 \rangle^{1/2} = (pd)^{1/5} L^{3/5}$, where p is the persistence length (which is proportional to the molecular stiffness), d is molecular diameter, and L is contour length of DNA [5]. For bacteriophage DNA in aqueous solution, R_g is typically on the order of a micron, which is barely large enough to image optically; the direct visualization of its interaction with proteins is therefore not possible with optical resolution. Although atomic force microscopy (AFM) can directly visualize small molecules with sub-micron length scale [6–8], AFM is incapable of providing information on the fast kinetics of DNA–protein interactions.

However, recent advances in single-molecule detection have enabled researchers to directly follow individual reaction pathways of molecules of interest in real-time [9–12]. Tools such as total internal reflection fluorescence microscopy (TIRFM) and charge-coupled-device cameras can be used to detect emission from a single fluorophore. In TIRFM, fluorescently labeled molecules are visualized by exciting fluorophores with an evanescent wave field that is created just above the surface separating two media having different refractive indices against which incident light is completely reflected. The intensity of the evanescent wave decays exponentially over a distance scale of a few hundred nanometers from the surface, thus eliminating the background fluorescence originating from outside the proximity of the reflecting surface. DNA molecules can easily be labeled with dyes that are known to intercalate between base pairs, while for visualization of proteins more careful methods are required to preserve their native catalytic activity. The motion of a fluorescently tagged protein may be more easily monitored on a stretched and

J. H. Kim and V. R. Dukkipati contributed equally to this work.

J. H. Kim · R. G. Larson (✉)
Department of Chemical Engineering, University of Michigan, Ann Arbor 48109, MI, USA
e-mail: rlarson@umich.edu

V. R. Dukkipati · S. W. Pang
Department of Electrical Engineering and Computer Science, University of Michigan, Ann Arbor 48109, MI, USA

immobilized DNA than on a coiled DNA, since along the former the protein follows a straight 1D path along the DNA. Stretching DNA is also useful if one wishes to monitor its interactions with proteins that are not fluorescently labeled, since the force needed to stretch the DNA (if it can be measured), can give information about the protein–DNA interactions. DNA is an elastic polymer whose force versus extension relationship is well described by the so-called worm-like chain (WLC) model [13, 14], and the information on the force applied to the DNA can be directly converted into extension, and vice versa.

Methods of stretching and immobilizing DNA molecules have been explored extensively over last decade in an attempt to develop DNA templates that meet the following requirements: (1) the stretched DNA molecules should preserve the base stacking structure of unstretched DNA, thus allowing normal DNA–protein interactions; (2) the DNA should be immobilized in such way that it is firmly held to withstand the hydrodynamic flow while providing ample space for proteins to move freely along the DNA; (3) the DNA should remain stretched and immobilized at physiological pH and salt concentrations. In the present report, we discuss published methods of DNA stretching and immobilization that can be categorized into one of three groups, based on the method of applying an external force onto the DNA. In the first group, force is exerted on one or both ends of the DNA molecule using optical and magnetic traps. This requires that DNA be end-modified with beads that are either optically refractive or magnetic so that they can be immobilized, respectively, by a laser beam or a magnetic field, respectively. The second group of DNA stretching and immobilization methods includes ''electrostretching,'' by which a high-frequency AC field is used to stretch DNA via a process that depends on molecular polarizability [15]. In electrostretching, DNA molecules are typically stretched between electrodes and anchored at one or both ends to the electrode.

The third group of methods for DNA stretching and immobilization (which may be the simplest) involves the use of flow fields. Flow can produce two kinds of forces that can stretch DNA molecules, namely, the viscous drag produced by the bulk flow surrounding the DNA, and the meniscus force created by an air–solvent interface moving along the DNA. The latter method, more commonly known as ''molecular combing'' [16, 17], often produces highly overstretched DNA molecules in which the bases are unstacked into a flat parallel ladder, and will be discussed in more detail in section ''Stretching by a moving interface.'' There are many ways in which flow fields can be generated to stretch and immobilize DNA molecules. For example, a microfluidic channel can be assembled using a polydimethyl siloxane (PDMS) scaffold or by fabricating silicon wafers [18, 19]. With microfluidic devices, sample volume can be reduced to a few tens of μLs, substantially reducing the cost of running assays. A novel method that we call protein-assisted DNA immobilization uses a flow field containing DNA-binding proteins to stretch and immobilize DNA molecules in a microfluidic device [19].

Here, we review the aforementioned methods of DNA stretching and immobilization and how these DNA molecules are used to investigate interactions with proteins at the single-molecule level.

Optical traps

Optical trapping of dielectric beads of size ranging from 10 μm to 25 nm was first demonstrated by Ashkin et al. [20] using a single-beam gradient force trap. Optical trapping relies on conservation of momentum which requires that a photon refracting through a transparent particle whose refractive index is higher than its surrounding medium produces a force on the particle due to a change in direction, and hence momentum, of the light. In practice, a laser beam is focused through a high numerical aperture microscope objective, creating forces on the particle in all directions. Two types of force, namely gradient and scattering forces, are produced since the laser light can be both transmitted and reflected from the particle. The gradient force is proportional to the gradient of intensity and is parallel to the intensity gradient while the scattering force is proportional to the optical intensity and is parallel to the incident light beam. The forces balance when the particle is centered at the point of maximum light intensity, and when the particle drifts from this position the resulting unbalanced force pushes the particle back into the center of focus of the beam. Hence the particle is trapped at the focal point of the laser, and the relationship between the displacement of the particle from the focal point and the applied force can be determined through a calibration procedure. This ''trapping potential'' then can be used to convert the measured bead displacement into the mechanical force exerted on the bead.

DNA molecules can then be manipulated by holding in an optical trap a polystyrene bead that is attached to one end of a DNA molecule and then stretching the molecule with a hydrodynamic flow or the second optical trap that pulls on a bead attached to the other end. Optical traps have been used to study polymer physics, using DNA as a model polymer that could be optically imaged. For example, the group of Steven Chu [21] visualized single tethered DNA molecules stretched in a uniform flow to investigate viscous forces and hydrodynamic interactions between the DNA molecule and the flowing fluid. By measuring the DNA length at different fluid velocities, they found that the fractional extension of the DNA (x/L, where x is the

projected length of the stretched molecule in the flow direction and L is the contour length of the DNA) scales with length as $L^{0.54\pm0.05}$. While this scaling law was expected for polymer coils, whose coil radius scales with L roughly this way, it was a surprise to find that the same scaling law seemed to apply even for nearly fully stretched molecules. Eventually, this result was explained by consideration of hydrodynamic interactions between different parts of the molecule and the relative insensitivity of these interactions to coil deformation [22].

Using an optical trap, Smith et al. measured DNA extension as a function of force on the DNA over the range 0–80 pN [23]. To do this, Smith et al. used λ-DNA linked at both ends to polystyrene beads, one of which was held by a stationary micropipette and the other by an optical trap, allowing the DNA to be stretched while monitoring the force (Fig. 1A) using the trap potential. At low external forces (< 10 pN), the DNA extension versus force curve can be well fitted by the WLC model. As the DNA chain is stretched towards it full contour length, the force abruptly rises and reaches a plateau value of ~65 pN, at which point the DNA abruptly overstretches to 170% of its B-form

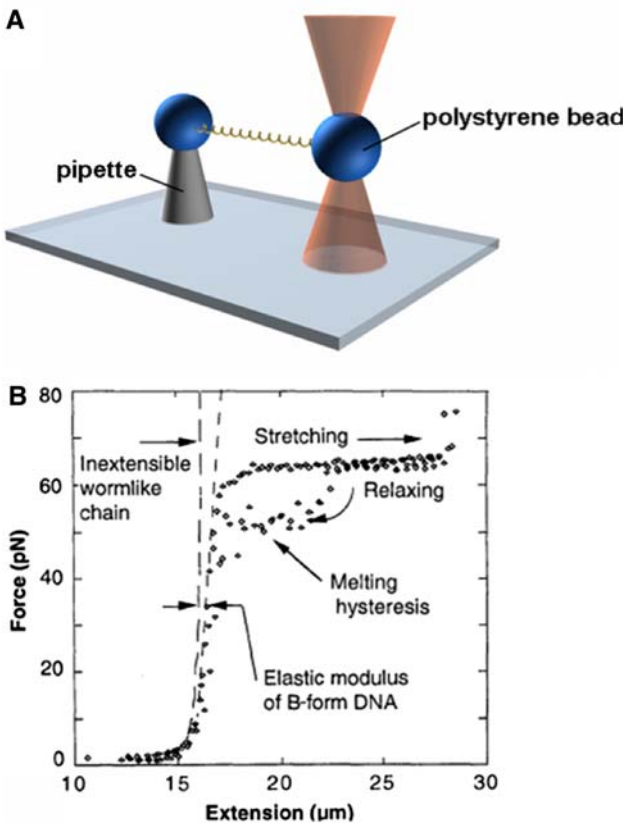

Fig. 1 (**A**) Schematic of experimental setup used in [20]. (**B**) Force versus extension for λ-DNA in 150 mM NaCl, 10 mM Tris, 1 mM EDTA, pH 8.0. Reprinted with permission from *Science* **271**, 795 (1996). Copyright 1996 by the American Association for the Advancement of Science

contour length (Fig. 1B). The first-order-like transition into the overstretched form of DNA (S-form) suggests that the transition occurs cooperatively, unstacking bases into a flat parallel ladder structure.

Beyond studying the physical properties of DNA, researchers have extensively studied the interactions between optically trapped DNA and proteins. RNA polymerase (RNAP), for example, is a motor protein powered by nucleotide triphosphate (NTP) hydrolysis during RNA synthesis based on information read from DNA. Yin et al. [24] measured the transcriptional velocity of *E. coli* RNAP against an applied force on a DNA by directly monitoring the displacement of a DNA molecule held by an optical trap as it is transcribed by an immobilized RNAP (Fig. 2A). As RNAP actively transcribes the DNA, the bead is pulled from the trap center, and a tension builds up on the DNA until the force exerted by RNAP balances that exerted by the optical trap. In this way, they showed that the RNAP generates a considerable force (> 14 pN) during transcription elongation.

Bustamante and coworkers investigated the effect of assisting and opposing forces on the transcriptional pausing and arrest of *E. coli* RNAP as shown in Fig. 2B [25, 26]. During transcription, *E. coli* RNAP is known temporarily to stop or ''pause'' its transcription elongation or in some cases undergo an irreversible structural change leading to a permanent halt or ''arrest'' of transcription. These pauses and arrests are deviations from the main elongation pathway, and play an important role in the regulation of gene expression. In their experiments, a ternary complex including DNA template, RNAP, and nascent RNA is stalled at a predetermined position, followed by immobilization of RNAP onto a bead surface which is optically trapped. Depending on the geometry of the complex, the buffer flow stretching the DNA can either assist or oppose transcription elongation (Fig. 2B). Pauses of RNAP seen during the transcription in assisting geometry are shown in Fig. 2C. Bustamante and coworkers found that the force either opposing or assisting the transcription elongation does not affect the transcriptional velocity. This is consistent with the results of Yin et al. who found that the transcriptional velocity is force-independent until the force is high enough to deactivate the protein, suggesting that mechanical translocation of RNAP is not a rate-limiting step in transcription elongation. Nevertheless, the force assisting the transcription elongation apparently decreases the pause frequency and increases both the mean transcription length and the fraction of pause-free transcription compared to the case where the force opposes transcription elongation, indicating that the entry into the pause state is force-dependent. However, the exit from the paused state is observed to be force-independent, suggesting that the transition state between the entry into and exit from the paused state is asymmetrically positioned in the reaction

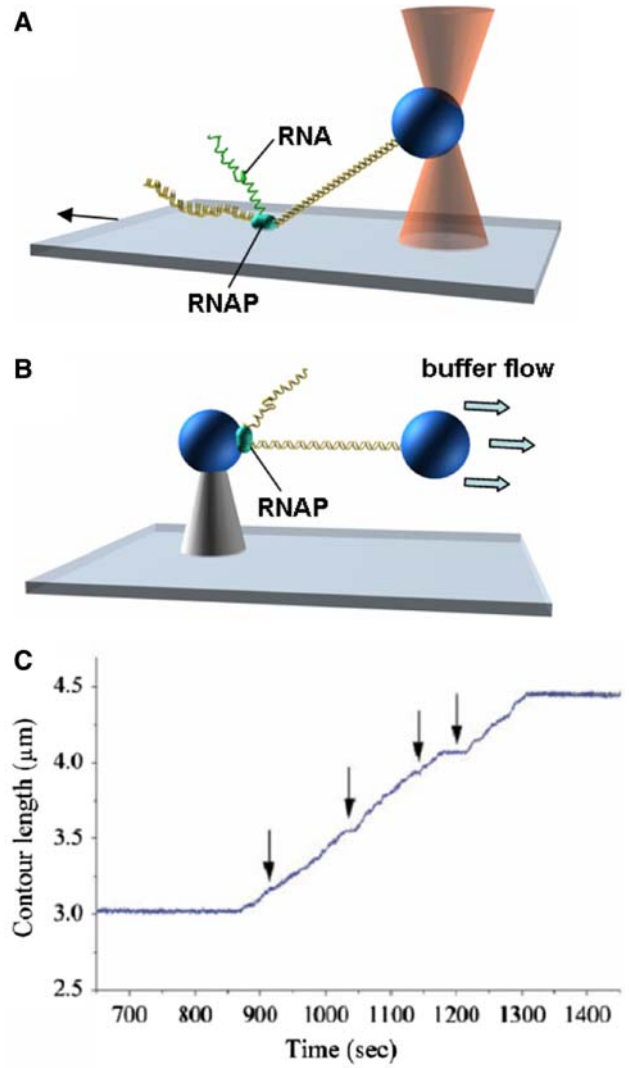

Fig. 2 Schematic representations of experimental setup used in (**A**) Ref. [24] and (**B**) Refs. [25, 26]. (**C**) The length between two beads changes as RNAP transcribes DNA under a force that assists forward transcription. Pauses during transcription are indicated by arrows. Reprinted from *Proc. Natl. Acad. Sci. USA* **99**, 11682 (2002). Copyright 2002 National Academy of Sciences, USA

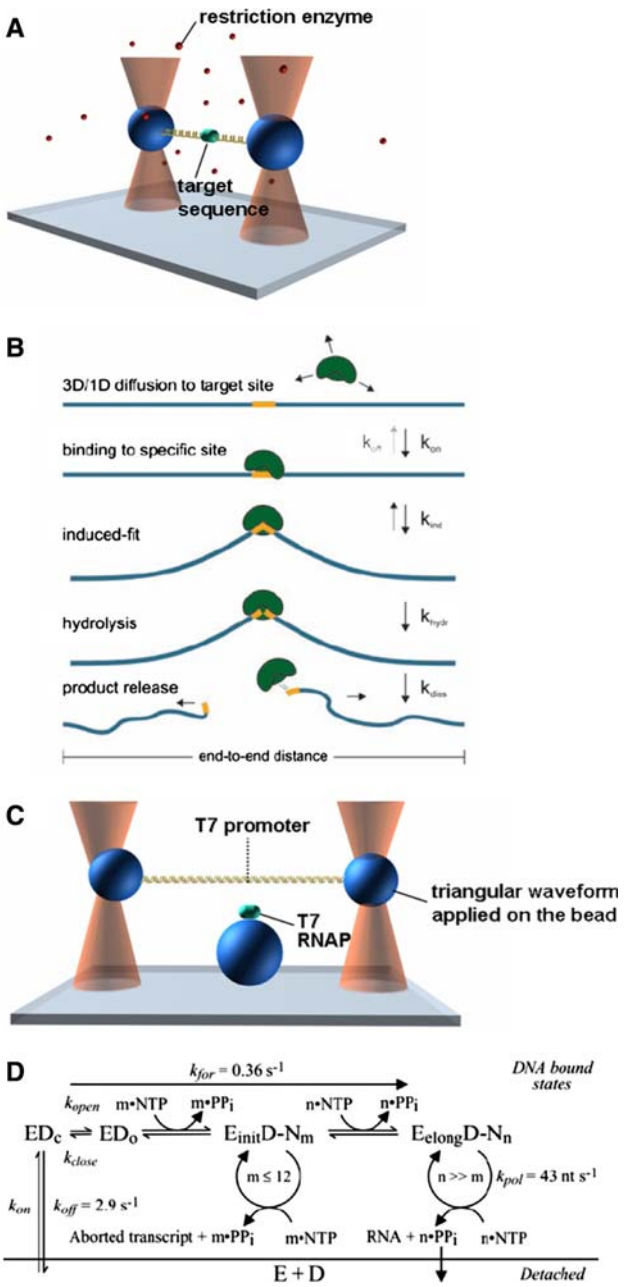

Fig. 3 (**A**) Schematic representation of experimental setup used in Ref. [27]. (**B**) The reaction pathway for type II restriction enzymes. The applied tension opposes DNA bending by the enzyme in the induced-fit process. Reprinted with permission from *Nucleic. Acids Res*. **32**, 3040 (2005). Copyright 2005 by Oxford University Press. (**C**) Schematic representation of experimental setup used in Ref. [28]. (**D**). Kinetic scheme for transcription by T7 RNAP. E denotes free enzyme state; D, DNA template; ED_c, DNA-bound closed complex; ED_o, DNA-bound open complex; $E_{init}D - N_m$, ternary complex engaged in abortive RNA synthesis; $E_{elong}D - N_n$, ternary complex engaged in elongation; PP_i, pyrophosphate. Reprinted from *J. Biol. Chem*. **279**, 3239 (2004). Copyright 2004 by the American Society for Biochemistry and Molecular Biology

coordinate, with one state energetically favored. Similar results have been observed with transcriptional arrests where the assisting force reduces the incidence of arrest, although the exit from the arrested state is rarely observed. These experiments elucidate details of the reaction pathways of prokaryotic transcription that are not available from conventional bulk studies.

Multiple optical traps can be used to grab one or more DNA molecules by their ends simultaneously. For example, van den Brook et al. [27] investigated the dependence of restriction enzyme activity on the tension exerted on DNA optically trapped at both extremities as shown in Fig. 3A. The tension on the DNA was controlled by moving the position of one of the optical traps while monitoring the force on the DNA with the other trap. Type II restriction enzymes *Eco*RV and *Bam*HI were used to

cleave the DNA at specific locations (''GATATC'' for *Eco*RV and ''GGATCC'' for *Bam*HI) which was registered by a sudden drop in the tension. This study showed that the cleavage rate for *Eco*RV decreases with DNA tension whereas that for *Bam*HI remains constant as long as the tension is not so high as to overstretch the DNA. The difference in the dependence of cleavage rate on the DNA tension could be traced to dissimilarity between two enzymes in the ''induced-fit'' reaction with DNA, with the tension-dependent enzyme significantly bending the DNA upon binding. Their results were consistent with the crystallographic images of the two enzymes bound to their cognate sequences wherein *Eco*RV strongly bends the DNA inside the binding pocket while *Bam*HI does not (Fig. 3B).

Using a dual optical trap setup, Skinner et al. [28] investigated promoter binding, initiation, and elongation of RNA by T7 RNAP. Bacteriophage T7 RNAP is a single subunit enzyme fully capable of transcribing DNA into RNA just as does the much more complicated eukaryotic RNAP. In the experiment of Skinner et al., an optically trapped DNA bearing a T7 promoter sequence was maneuvered to interact with T7 RNAP immobilized to a bead on a glass coverslip by applying a triangular waveform displacement on one of the traps, while monitoring the coupled motion of the other bead (Fig. 3C). The RNAP–DNA interaction was identified through changes in the ''stiffness'' of the response of the second bead to motion of the first. In this way, they measured the lifetime of T7 RNAP bound to the promoter, from which they could obtain the dissociation rate constant k_{off}. In some DNA-binding events that lasted much longer than others, a clear movement of one of the beads toward the surface-bound bead against the optical restoring force was observed. The rate at which the distance between these two beads decreased corresponded to the transcriptional velocity k_{pol}. They could also directly measure the duration of the lag between transcriptional initiation and elongation by measuring the time between onsets of the DNA-binding and unidirectional bead movement corresponding to the transcriptional elongation. The stationary complex may represent a ternary complex engaged in abortive RNA synthesis in which a short RNA chain of length 7–12 nt is repeatedly released. The forward rate k_{fow} at which the closed complex transitioned to the elongation complex could be obtained using the measurements of lag times (Fig. 3D).

Magnetic traps

Magnetic traps operate similarly to optical traps in that they allow free maneuvering of a bead in solution. Just as a particle is trapped in a potential well created by the laser intensity profile in an optical trap, the force generated by an electromagnetic field gradient traps a magnetic particle. Typically, one end of the DNA molecule is fixed on a surface while the other end, to which the magnetic bead is attached, is held by the magnetic trap in solution (Fig. 4). The force on the DNA, which can be varied by changing the distance between the magnet and the bead, typically ranges from tens of fN to ~100 pN. The extension of the DNA in the vertical direction (l) can be measured by analyzing the bead image using a diffraction ring whose diameter increases with the distance of the bead from the focal plane. The magnetic force on the DNA can be computed using the equipartition theorem in which the force is expressed as $F_{\text{mag}} = k_{\text{B}}Tl/\langle \delta x^2 \rangle$, where δx is the transverse Brownian fluctuation of the bead [29].

In early experiments with magnetic traps, Smith et al. [30] studied the elasticity of single DNA molecules by measuring the DNA extension as a function of external force. In their setup, one end of the DNA was chemically attached to a surface and the other end to a magnetic bead held by the magnetic trap. The DNA was forced to stretch upward by a hydrodynamic flow and was simultaneously pulled to the right by the magnetic trap, creating an angle θ relative to the horizontal axis. The tension on the DNA was calculated from the measured values of F_{mag} and θ. They found that the extension versus force curve for a double stranded DNA molecule deviates from the prediction of the freely jointed chain (FJC) model, which assumes that the Kuhn segments are uncorrelated in the absence of external forces. A more precise description of the DNA elasticity was provided by taking into account the continuous rigidity of the polymer chain through the inextensible WLC model, although this model fails to describe the DNA under tensions greater than 10 pN. Marko later proposed an extensible WLC model that also includes twisting elasticity as a

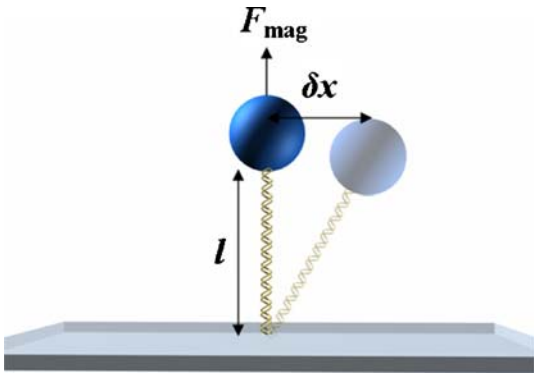

Fig. 4 Schematic representation of the force measurement. The magnetic force applied to the bead stretches the DNA vertically. The transverse Brownian fluctuation of the bead δx is used to calculate the force using the equipartition theorem in which the force is expressed as $F_{\text{mag}} = k_{\text{B}}Tl/\langle \delta x^2 \rangle$

model for DNA that can be applied to DNA under high tensions [31].

Bensimon and coworkers have pioneered the study of DNA–protein interactions using magnetic traps. In one of their experiments, Maier et al. [32] measured the real-time replication rate of a single DNA polymerase (DNAP) on a single-stranded DNA (ssDNA) stretched by a magnetic trap as shown in Fig. 5A. Similarly to RNAP, DNAP reads the base sequence information from a single-stranded template and synthesizes the complimentary strand. The differences between DNAP and RNAP include (1) catalyzing of addition of a new deoxyribonucleotide triphosphate (dNTP) to the growing chain of DNA for DNAP while RNAP catalyzes the addition of NTP to the growing chain of RNA; and (2) DNAP requires a primer (a short piece of ssDNA annealed to the template strand) to initiate the synthesis while RNAP does not. Maier et al. tracked in real-time the progress of replication by measuring the change in the elastic response to an external force that occurs as ssDNA is converted to double-stranded DNA (dsDNA) (Fig. 5B). At low forces (< 5 pN), the elasticity of dsDNA can be well described by the WLC model as mentioned in the previous section, while that of ssDNA exhibits a complex behavior due to the secondary structure which varies with ionic strength and base composition. In the low force regime (< 5 pN), a higher force is required to stretch ssDNA than to stretch dsDNA to the same extent, while a crossover occurs at a force of ~5 pN. The extension versus force behavior of a partially replicated DNA is intermediate between ssDNA and dsDNA, which can be well described by the superposition of the elastic behavior of ssDNA and dsDNA. In this way, the DNA extension is converted into the number of dNTP incorporated into the growing DNA chain. Two different DNAPs were used in their experiments, both of which exhibit frequent pauses during the synthesis and show a decrease in the replication rate when the force exceeds 4 pN. The decrease in the replication rate is attributed to the work that DNAP has to perform against the external load to contract the template in order to fit it into the dsDNA structure during the polymerization rate-limiting step. We note that a similar experiment has been carried out using an optically trapped DNA molecule [33].

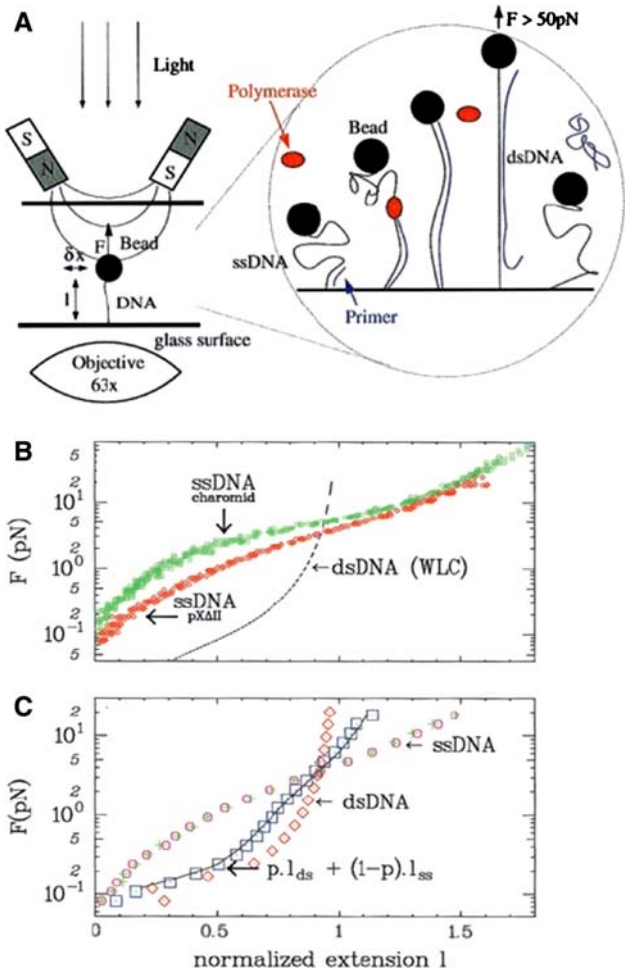

Fig. 5 (**A**) Schematic representation of experimental setup used in Ref. [32]. The magnets pull on the bead with a force $F_{mag} < 100$ pN. A primer is hybridized to the ssDNA for DNAP to initiate replication. As DNAP progresses, the molecule's extension increases due to the difference in the elastic behavior between ssDNA and dsDNA. The stretching force is increased to 50 pN to separate the newly synthesized strand from the template strand by destabilizing the DNA. (**B**) Comparison of the elasticity of a charomid and pXΔ II ssDNA and the WLC model curve for dsDNA. The difference in G + C content in ssDNA molecules influences the stability of secondary structure at low forces. (**C**) The force versus extenstion curve of a partially replicated DNA (squares) is intermediate between ssDNA (*circles*) and dsDNA (*diamonds*). The full line $l_p(F) = pl_{ds} + (1-p)l_{ss}$ is the superposition of elastic behavior of ssDNA and dsDNA at a percentage of replication of $p = 0.7$. All figures reprinted from *Proc. Natl. Acad. Sci. USA* **97**, 12002 (2000). Copyright 2006 by National Academy of Sciences, USA

Bensimon and coworkers [34] followed in real time the interaction between a type II DNA topoisomerase (topo) and dsDNA that had been stretched and supercoiled by a magnetic trap. Type II topo is an ATP-dependent protein that relaxes positive supercoiling by removing two supercoils per cycle to ensure proper segregation of DNA into daughter chromosomes. Supercoiling of DNA can be introduced simply by rotating the magnet above a surface-anchored un-nicked DNA molecule. The torque on the DNA builds up until it reaches the critical value at which the DNA buckles, forming a plectoneme (Fig. 6A). The DNA contracts in length by $\delta(\delta = 45$ nm per turn at a constant force of $F_{mag} = 0.7$ pN) as more positive supercoils are generated by the continued twisting of the DNA (Fig. 6B). As topo II is added to the system at low ATP concentration, the stepwise DNA extension by 2δ can be observed each cycle in which the protein removes two supercoils (Fig. 6C).

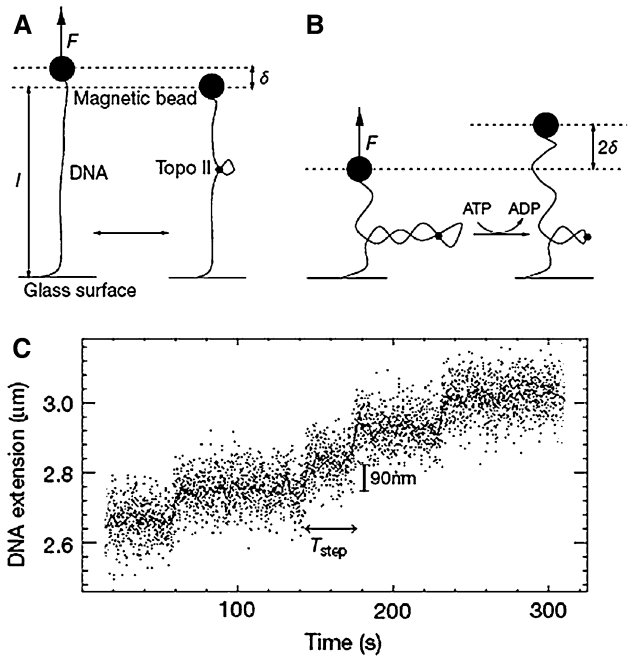

Fig. 6 (**A**) Schematic representation of the buckling instability of dsDNA undergoing topo II- mediated clamping in the absence of ATP. Topo II can stabilize the DNA supercoil by binding to the crossover between two DNA segments in the absence of ATP. (**B**) The relaxation of supercoils in the presence of topo II and ATP. Two supercoils are removed in each enzymatic cycle, resulting in an increase in the DNA extension by 2δ. (**C**) Individual steps of increase in the DNA extension are observed. All figures reprinted with permission from *Nature* **404**, 901 (2000). Copyright 2000 by Nature Publishing Group

Electrostretching

Stretching and immobilization of DNA in solution can also be performed by applying AC fields using microfabricated electrodes. Spatially non-uniform AC fields lead to molecular movement induced by polarization, which is known as dielectrophoresis (DEP). Depending on their polarizability relative to the solvent in which they are immersed, molecules tend to migrate towards either the highest field strength (positive dielectrophoresis) or the lowest (negative dielectrophoresis) [35]. Long polymers not only migrate but also align or stretch in the AC field, due to the tendency of the segments of polymer to align in the field, since unaligned segments experience an electric-field-induced torque acting on the induced dipoles [36]; i.e., a dielectric torque. Orientation due to this dielectric torque is sometimes also called ''dielectrophoresis,'' but here, to avoid confusion, we will restrict the term ''di-electrophoresis'' to migration in an AC field due to spatial gradients in the field. In addition to dielectric forces, such experiments can also induce electrothermal force acting on the fluid, whereby each electrode induces a circulatory fluidic motion across the electrodes [35]. This field-induced flow in turn contributes to DNA stretching [37]. In order to overcome the random thermal forces experienced by the DNA in solution, the electric field required for stretching is typically very high (around 10^6 V/m), which, however, can easily be generated using microfabricated electrodes, since gaps between electrodes are then very small. Often in such experiments, one end of the DNA molecule is first immobilized on one electrode followed by stretching the other end by the AC field.

Washizu and Kurosawa [15] were the first to demonstrate DNA immobilization and stretching using an AC electric field in deionized water (conductivity 2 μS/cm). They used microfabricated aluminum electrodes deposited and patterned on glass to manipulate λ-DNA molecules. The DNA molecules were covalently attached to the aluminum electrodes by an electrochemical process [38]. After attachment, the DNA molecules were stretched using a 1 MHz field. A floating electrode configuration was used to minimize the electrothermal force generated along the electrode edge, thus enabling the DNA molecule to attach to the electrode.

Namasivayam et al. [39] demonstrated DNA stretching in a microfluidic channel using non-uniform electric fields. Tris–HCl medium mixed with 3.75 wt% linear polyacrylamide was used to enhance DNA stretching [40]. The DNA molecules were found to stretch partially at around 1 KHz and also to stretch more fully at around 1 MHz. The existence of significant stretching at both these frequency ranges has been attributed to two distinct time constants governing relaxation of the counterion cloud present around the DNA molecule, one of these constants governing the tight ''Stern'' layer and the other the diffuse layer [41]. However, in the presence of an entangled polymer solution, additional mechanisms of stretching may be possible, due to ''reptation'' of the DNA through the polymer matrix [40]. Namasivayam et al. immobilized DNA molecules onto gold electrodes at 1 KHz using a thiol group bound to the 3′ end of the DNA. After attachment, the DNA was stretched and immobilized at the other end across a 20 μm electrode gap using 1 MHz AC field as shown in Fig. 7.

In subsequent work, Sung et al. [42] used a similar setup to study the efficiency of DNA stretching for different surface conditions and electrode designs in deionized water (pH 8.0, conductivity 2 μS/cm) mixed with 4 wt% polyacrylamide solution. They applied 1 KHz AC fields to attract the DNA molecules to the electrode's edge (apparently due to positive DEP) to enable DNA–thiol attachment to the gold electrode. After immobilization the DNA molecules were stretched and anchored at the other end using a 1 MHz field. The stretching that occurred at 1 MHz might have arisen either by a negative DEP or a flow that induced stretching.

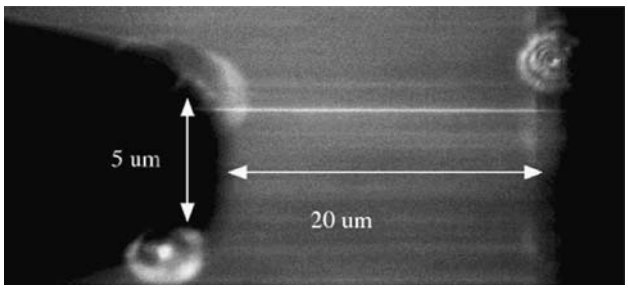

Fig. 7 Single λ-DNA molecule immobilized and stretched across 20 μm electrode gap using AC field (1 MHz, 3×10^5 V/m), in a linear polyacrylamide solution. Reprinted with permission from *Anal Chem*. Copyright 2002 by American Chemical Society

From these experiments, Sung et al. deduced that more efficient DNA stretching can be carried out with hydrophobic surfaces and thin electrodes than with those used in the experiments of Namasivayam et al. The physical phenomena behind DNA stretching for different frequencies, pH and conductivity of buffer, electric field strength and distribution, and the enhancement of stretching by polyacrylamide, are still not clear. Currently there are no equations that can describe the behavior of DNA stretching under different conditions [43]. The different forces and their influence on DNA stretching have yet to be fully understood.

Germishuizen et al. [44] conducted DNA stretching experiments (without added polymer) with a parallel electrode pair to study different forces that contribute to DNA stretching. DNA molecules were immobilized at one end to a gold electrode using a multi-step procedure involving biotinylation, thiolation and hybridization. The stretching of DNA molecules of different contour lengths was studied at various frequencies in deionized water (conductivity 1 μS/cm). They found that DNA stretching at first increases, and then decreases with increasing frequency as shown in Fig. 8. The maximum elongation was observed around 200–300 KHz for all different DNA fragments while no stretching was observed at frequencies below 100 KHz or above 1.1 MHz. The decreased stretch lengths at higher frequencies could be due to an inability of the DNA segment dipoles to respond at the highest frequencies. The same study showed that the normalized stretch was independent of the contour length and the position of the segment of interest, i.e., the distance from the electrode. From the above results and experiments conducted with an electric-field-induced fluid flow at different frequencies, the authors concluded that both the field-induced segment orientation due to dielectric torque and the induced flow contributed to the DNA stretching, whereas the dielectrophoretic force produced by the field gradient had little influence. Further experiments conducted with varying electrode gaps

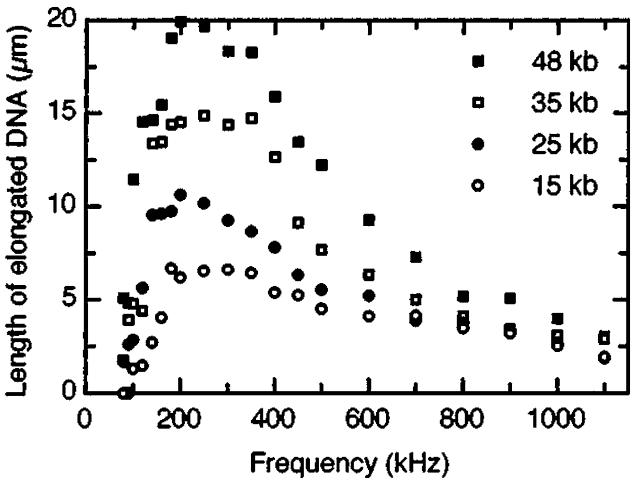

Fig. 8 Stretch length of elongated DNA as a function of frequency at an electric field of 0.5 MV/m across a 40 μm gap; 48 kb (closed squares), 35 kb (*open squares*), 25 kb (*closed circles*), and 15 kb (*open circles*). Reprinted with permission from *J. Appl. Phys*. **97**, 014702 (2005). Copyright 2005 by American Institute of Physics

showed that DNA molecules can only be elongated to half the electrode gap if the DNA contour length is longer than the electrode gap.

Walti et al. [37] studied DNA stretching by recording images both parallel and perpendicular to the plane of the electrode, and concluded that the major contribution to stretching is from the AC-field-induced dielectric torque while the directionality of stretching is provided by the electric-field-induced flow. They argued that the dielectric torque tends to align molecular segments but cannot on its own produce stretching, since the segments will align equally both parallel and anti-parallel to the field, unless a bias is introduced. The field-induced flow is one source of a bias. To stretch the DNA, the induced flow has to be directed from the electrode edge towards the gap. Also, DNA molecules with contour length greater than half the electrode gap cannot be stretched beyond the center of the gap because the electric-field-induced fluid flow from both electrodes changes direction midway between the gaps. DNA molecules cannot stretch in a direction opposite to the induced flow. However, for high fields, Cohen [36] pointed out that the dielectric torque can produce full stretching, since there is a bending energy associated with each ''kink'' where the DNA alignment changes direction, and this bending energy is only eliminated when the kinks disappear, and the molecule is then fully stretched. Thus, there is not necessarily a need for a ''bias'' to produce full stretching of DNA by dielectric torque.

DNA molecules can also be immobilized to gold electrodes by preparing the DNA solution in a weak acidic buffer (pH 5.5–6.6). The DNA becomes ''sticky'' at the

ends at low pH conditions due to protonation of bases leading to the exposure of hydrophobic core as will be discussed more in detail in section ''Stretching by a moving interface.'' Using these DNA molecules, the immobilization and stretching can be performed in a single step without any chemical modifications to either the electrode or the DNA. Dukkipati et al. [45] have demonstrated DNA stretching and immobilization in microfluidic channels in acidic condition (pH 5.8) and non-uniform electric fields. When the electric field is applied across the electrode gap below 8 V, DNA molecules are carried by the electrothermal fluid flow and attach to the gold electrode as shown in Fig. 9. At higher than 8 V, the induced fluid flow reverses direction from the electrode edge toward the gap for both electrodes) such that DNA molecules stretch from both sharp- and straight-edged electrodes as shown in Fig. 9C.

Electrostretching of DNA molecules has been used to aid the study of the motion of DNA-interacting proteins along the DNA molecule. Kabata et al. [46] have directly observed fluorescently labeled *Eco*RI proteins sliding under convective flow along electrostretched DNA molecules held between electrodes. In these experiments, sliding along the DNA was distinguished from simple convection in the flow by a change in direction of the motion of the stained proteins when they encountered the DNA molecules. One possible future application of stretching DNA molecules across electrode gaps is a fabrication of a network of DNA-templated carbon nanotube (CNT) transistors to realize fully functional digital blocks such as inverters and adders [47]. In the construction of these CNT transistors, electrostretching may be of advantage in that it allows placement of stretched DNA molecules at precise locations across electrodes [45], as opposed to DNA combing, in which DNA placement is random. We will discuss combing in more detail in section ''Stretching by a moving interface''.

Flow stretching

Stretching by hydrodynamic drag

As mentioned in the section ''Introduction,'' stretching and immobilization of DNA using flow occurs either by hydrodynamic drag or the action of a moving meniscus. In this section, we discuss methods that use hydrodynamic drag. We have already described a couple of experiments that used a hydrodynamic buffer flow to stretch the free end of a DNA molecule anchored at the other end by an optical or a magnetic trap. In this section, we discuss experiments in which the DNA is attached to a surface at one end by an avidin–biotin linkage and is free in solution at the other end (Fig. 10A). Avidin is a tetrameric protein each subunit of which provides a strong binding site for a biotin molecule. A monolayer of avidin can deposited directly onto an acid-cleaned glass surface [3], or onto either a monolayer of biotin-labeled BSA [48] or a biotin-poly(ethylene glycol) brush, which is known to reject non-specific binding of proteins [49, 50]. The biotin labeling of the DNA is generally carried out by annealing a biotin-modified oligonucleotide to the DNA. As discussed earlier, the force on the DNA can be obtained from the transverse Brownian motion of the free end of the DNA using the equipartition theorem.

van Oijen et al. [14] observed the digestion by λ exonuclease of dsDNA into ssDNA at the single-molecule level. λ exonuclease degrades each strand of duplex DNA in the 5′ to 3′ direction by means of hydrolysis of phosphodiester bonds in a highly processive manner. In each enzymatic cycle, λ exonuclease catalyzes the hydrolysis of a phosphodiester bond, translocates along the DNA, and melts the 5′ terminal base from neighboring bases. Three oligos were annealed to the DNA to ensure that modifications in extremities to provide binding sites for avidin and microsphere occur at one strand only, leaving the other 5′ terminus exposed to initiate the digestion. As in the

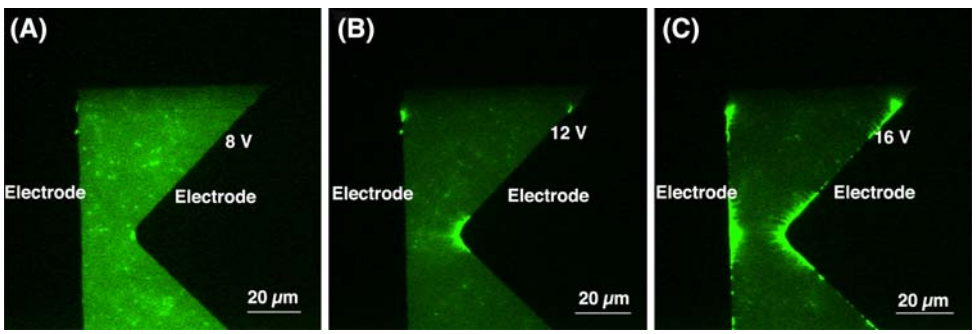

Fig. 9 DNA stretching for different voltages at 100 KHz in a 100 μm wide and 75 μm deep Si microchannel. (**A**) DNA stretching starts at the tip of pointed electrode at 8 V. (**B**) Greater numbers of stretched DNA molecules covering a greater area are observed near the tip of the pointed electrode at 12 V. (**C**) DNA molecules stretched at both the straight edge and pointed electrodes at 16 V. Reprinted with permission from *Appl. Phys. Lett*. **90**, 083901 (2007). Copyright 2007 by American Institute of Physics

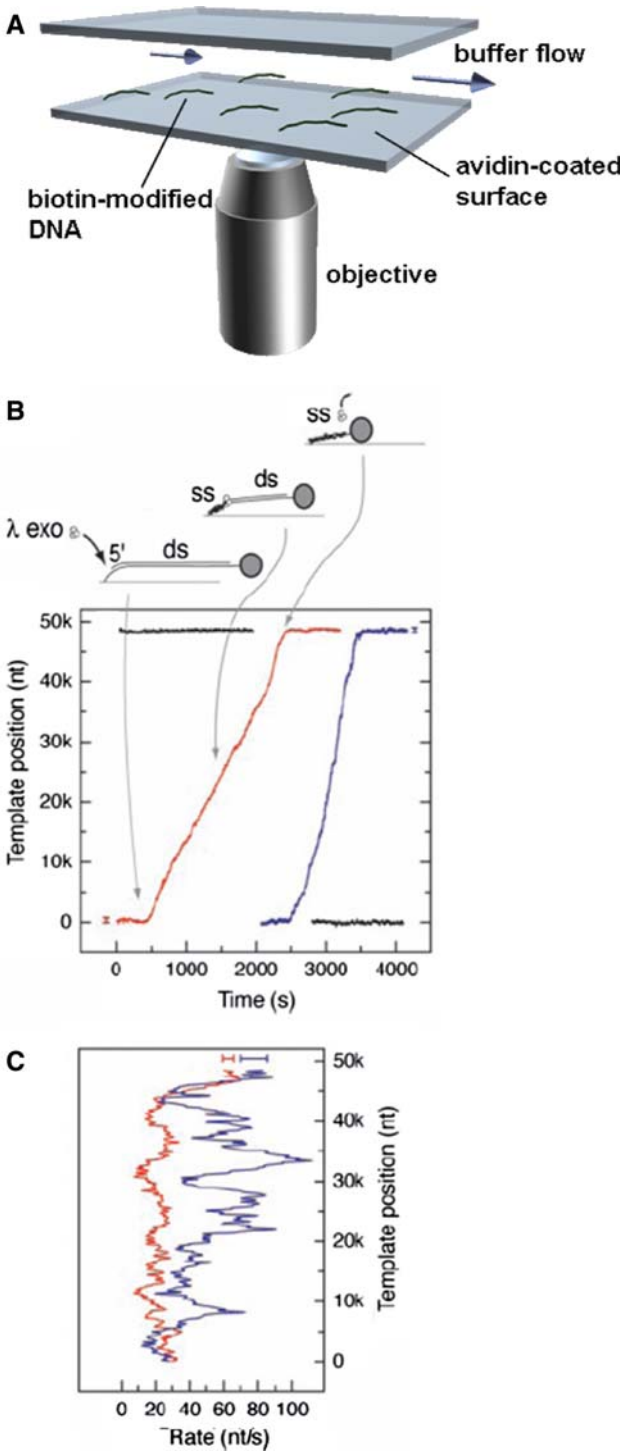

Fig. 10 (**A**) Schematic representation of the experimental setup in which biotinylated DNA is immobilized at one end to an avidin-coated surface while the free end is stretched by buffer flow. (**B**) Two digestion trajectories showing complete conversion of dsDNA into ssDNA by λ exonuclease. Two black traces correspond to beads tethered to ssDNA (*top*) and dsDNA (*bottom*). (**C**) Time derivatives of the two trajectories in (**B**) as a function of template position. Figures in (**B**) and (**C**) are reprinted from *Science* **301**, 1235 (2003). Copyright 2003 by the American Association for the Advancement of Science

experiments of Maier et al. presented in the previous section, the transition from dsDNA to ssDNA is detected by monitoring the elastic response to low stretching forces (<6 pN). van Oijen et al. observed the decrease in the DNA length as λ exonuclease specifically degrades one strand of the dsDNA (Fig. 10B). The digestion rate exhibits large fluctuations depending on the position along the DNA template, suggesting that a sequence-dependent melting of the base pair (bp) is the rate-limiting step in the enzymatic cycle (Fig. 10C).

Blainey et al. [51] observed the 1D Brownian motion of human oxoguanine DNA glycosylase 1 (hOgg1) along similarly flow-stretched DNA. DNA glycosylases initiate DNA repair by catalyzing excision of damaged bases and hOgg1 in particular removes highly mutagenic base 8-oxoguanine from the human genome. The protein has to locate these damaged bases amidst the vast number of native bases and the question of how these DNA-binding proteins locate their target sequence has long remained unanswered. It has been proposed that proteins reach their target sequence in part by a facilitated diffusion along the contour of the DNA [52, 53]. The mechanisms of facilitation could include 1D ''sliding'' of proteins along the DNA contour and short range ''hopping'' or long range ''jumping'' of proteins through 3D space from one site to another on the DNA. The DNA was attached to a surface at one end by avidin–biotin linkage while the other end was free in solution. The protein was fluorescently labeled with Cy3B at the C-terminal engineered cysteine. When these proteins were introduced into a flow cell by a strong shear flow which also stretched the DNA on the surface, Blainey et al. observed the 1D movement of single proteins along the DNA (Fig. 11A). These proteins exhibited a typical 1D Brownian motion in which the net displacements were symmetric around zero. The 1D diffusion coefficients (D_1) were obtained by plotting the mean-square displacements (MSD) as a function of time at various salt concentrations. Varying the salt concentration is expected to influence the protein diffusion by changing the non-specific binding affinity if the search mainly occurs through 3D space. However, the D_1 values obtained in their experiments exhibited no dependence on salt concentrations despite the apparent decrease in binding lifetimes (Fig. 11B), suggesting that during the sliding the protein maintains registry with the DNA, and does not hop on and off, since the rate of re-binding to the DNA should be affected by salinity. These results demonstrate how single-molecule techniques can be used to characterize directly molecular properties that could not have been measured with conventional bulk studies.

Our group and others have also stretched DNA molecules in a flow generated by drying a droplet deposited onto a positively charged surface such as one treated with

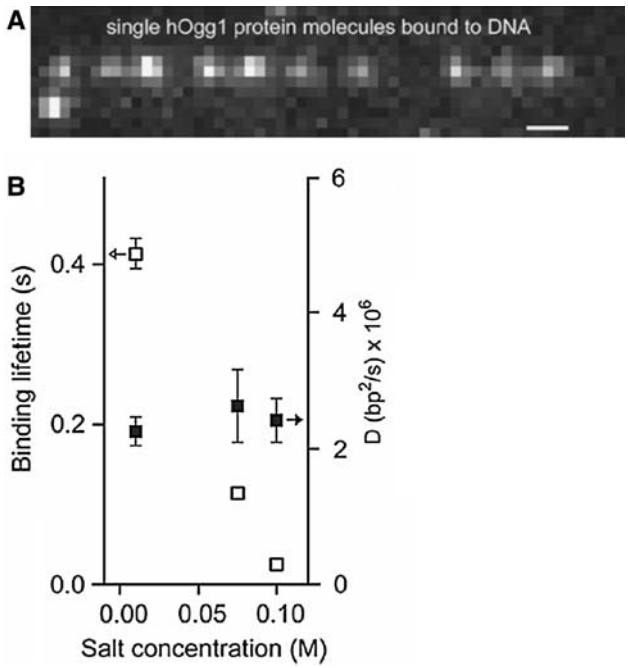

Fig. 11 (**A**) Image of single hOgg1 protein molecules bound to flow-stretched λ-DNA. Scale bar = 1.0 μm. (**B**) Mean binding lifetime (*open symbols*) and 1D diffusion coefficient (*closed symbols*) as functions of salt concentration. All figures reprinted from *Proc. Natl. Acad. Sci. USA* **103**, 5752 (2006). Copyright 2006 by National Academy of Sciences, USA

aminopropyltriethoxy silane (APTES) [54, 55]. When the contact line is pinned to this surface, a radial flow is created to replenish fluid that is evaporated from the periphery of the droplet [56]. This flow both transports DNA molecules towards the periphery and stretches them. Since the DNA is negatively charged along the backbone, it sticks to the positively charged APTES surface via electrostatic interactions, or, more precisely, it adheres to the surface due to the entropy gained by releasing counterions. Jing et al. [54] and Chopra et al. [55] have reported the deposition of λ DNA molecules onto an APTES-treated surface via a drying droplet flow. Brownian dynamics simulations using a bead-spring representation of the DNA molecule predict 22% stretching for DNA molecules adsorbed near the edge of the droplet (i.e., at radial positions greater than 90% of the droplet radius) for droplets dried under relatively ''fast'' evaporation conditions (i.e., low humidity), which agreed with the experimental findings (Fig. 12). This stretch is much poorer than in meniscus-force-driven stretching. From the simulations, one can infer that this rather poor stretching is due to the downward convective flow created inside the drying droplet which tends to push DNA molecules onto the surface before they get chance to fully unravel.

Although these DNA molecules are not in general fully stretched, they are a good template for an optical mapping application. DNA molecules that are stretched and firmly immobilized onto a surface can be cleaved by type II restriction enzymes at one or more positions along the backbone. As mentioned in the previous section, type II restriction enzymes cleave both strands of the DNA by recognizing a specific sequence on the DNA and catalyzing the hydrolysis of phosphodiester bonds. In order to optically locate the positions of cleavage, it is desirable that the cleaved fragments be retained in their original locations. Jing et al. [54] have demonstrated the enzymatic cleavage of λ-DNA molecules that were stretched and immobilized onto an APTES-treated surface by drying droplet flow. The DNA fragments were well preserved on the surface as shown in Fig. 13.

Stretching by a moving interface

Bensimon and coworkers developed a simple, but very clever, method to stretch and align large number of DNA molecules onto a hydrophobic substrate by the action of a receding water meniscus [16, 17]. This so called ''molecular combing'' method is carried out as follows: (1) the DNA is dissolved in a buffer solution at pH 5–7, slightly below the physiological pH in order to slightly denature DNA at its the ends; (2) a hydrophobic substrate is dipped into a the DNA-containing solution; and (3) the substrate is slowly pulled out of the solution, leaving highly aligned DNA molecules firmly attached to the substrate (Fig. 14A). In this remarkably simple method, the stretching and anchoring of the DNA is believed to come about in the following way. First, a free end of the DNA sticks to the hydrophobic substrate, presumably due to its affinity to the exposed hydrophobic bases at the end of the DNA; then the DNA molecule is stretched out by the force exerted on the rest of the DNA by the receding meniscus; and finally the other end also sticks to the substrate as it dries. The process results in a high-throughput alignment of DNA molecules. However, the force exerted on the DNA by the receding water meniscus is strong enough to ''overstretch'' the dsDNA by as much as 60% beyond the length of its physiological B-form helix, and the DNA molecules often stick to the substrate at multiple points along the backbone, limiting their ability to interact with proteins. Our group has recently demonstrated that the number of anchor points along the DNA backbone can be controlled by varying the pH [57]. At physiological pH the DNA bases are not locally melted and the adsorption occurs primarily at its ends, reducing the chances for attachment at other points along the DNA backbone. This also leads to a higher, more uniform stretch at this pH, apparently because avoidance of these interior attachment points removes ''anchor points'' that are present at lower pH and inhibit transmission of the meniscus force to the entire DNA molecule (Fig. 14B). The stretching can be further enhanced by using surfaces

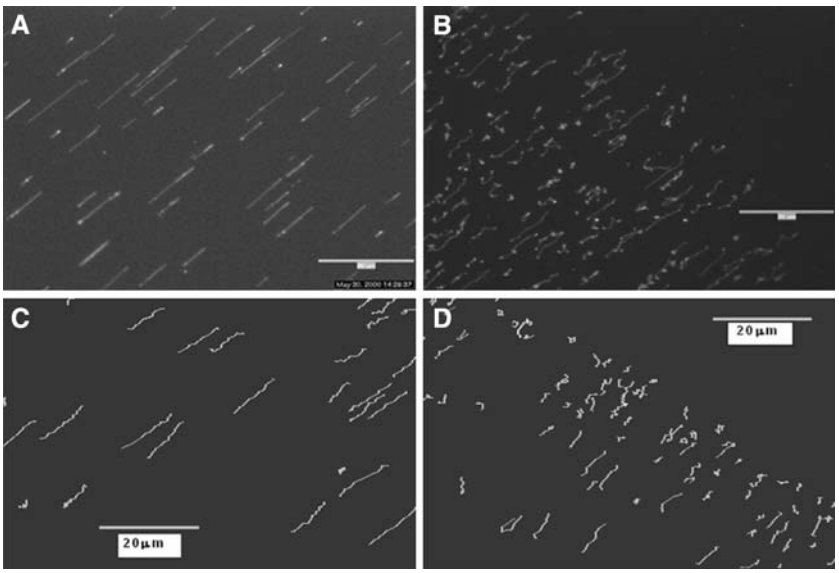

Fig. 12 DNA images at the edge of a droplet (radial position > 90%) at (**A**) a high evaporation rate (3 min drying time) and (**B**) a low evaporation rate (6 min drying time). (**C**), (**D**) Simulated DNA images under conditions identical to those in the experiments in (**A**) and (**B**), respectively. Scale bars = 20 µm. All figures reprinted with permission from *J. Rheol*. **47**, 1111 (2003). Copyright 2003 by the Society of Rheology

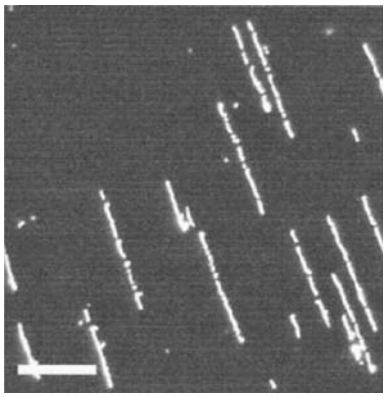

Fig. 13 Image of λ-DNA molecules stretched and immobilized on the APTES surface, digested with *Ava*I restriction enzyme. Reprinted from *Proc. Natl. Acad. Sci. USA* **95**, 8046 (1998). Copyright 1998 by National Academy of Sciences, USA

with low hydrophobicity which have reduced non-specific interactions with the DNA.

Gueroui et al. [4] have demonstrated that the overstretching of DNA can be suppressed by reducing the surface tension at the air/solution interface using a monolayer of fatty alcohol. In this way, they have deposited non-overstretched DNA molecules onto a hydrophobic substrate which served as a template for T7 transcription system. Gueroui et al. also visualized transcription on single combed T7 DNA molecules by using fluorescently labeled uridine triphosphate (UTP). This fluorescent monomer is incorporated into the growing RNA chain, generating a fluorescence signal as T7 RNAP transcribes the combed DNA to synthesize RNA. These RNA transcripts are visualized as bright dots aligned linearly on top of combed DNA (Fig. 14C). The RNAP–RNA transcript complex translocates along the DNA until it encounters an anchor point at which the DNA is attached to the surface. At this point, the protein complex stops and accumulates on the DNA as suggested by multiple fluorescent dots when multiple transcription initiation is allowed. When RNase T1, which degrades RNA in its coiled form, is introduced in the system, the bright dots are eliminated, suggesting that the RNA is not hybridized to the DNA.

Combed DNA molecules can also be used for ''optical mapping,'' which is a method devised by Jing et al. [54] of quickly locating endonuclease restriction sites along DNA molecules at optical resolution, and is useful for providing a ''scaffold'' for assembling DNA ''shotgun'' sequence data on small fragments (~1,000 bps) into a continuous sequence for a long DNA molecule. Although DNA molecules are frequently overstretched during combing, we find that the stretched lengths have a wide distribution when combed at low pH conditions as compared to the more uniform length distribution obtained for combing at physiological pH condition. As mentioned above, we believe that this is because combing at low pH conditions results in multiple anchor points along the backbone that prevent the meniscus force from being fully transmitted to the DNA [57]. However, the possible contribution of DNA breakage to the distribution of DNA stretch lengths is difficult to rule out. Since a large number of DNA molecules are stretched and deposited in a single run, we expect in each run to find a number of non-overstretched molecules capable of interacting with a restriction enzyme. To carry out the optical mapping, we simply comb YOYO-1 stained DNA molecules onto a hydrophobically treated cover glass, deposit a drop of *Eco*RI solution on top of this, incubate the solution in the dark for 20 min, and then illuminate and image the DNA quickly, to avoid photocleavage. *Eco*RI recognizes and cleaves DNA at the

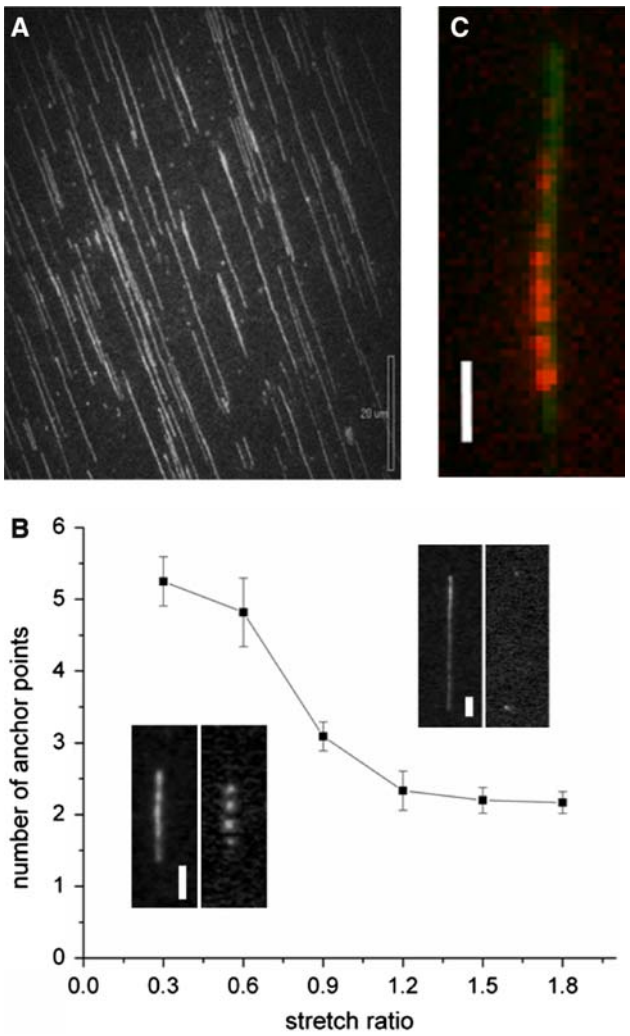

Fig. 14 (**A**) λ-DNA molecules combed onto a poly(styrene)-coated surface at pH 5.5. (**B**) The number of anchor points as a function of stretch ratio (*x*/*L*, where *x* is the stretched length and *L* is the DNA contour length) for T7 DNA molecules stretched at pH 8.0 on a poly(methylmethacrylate)-coated surface, measured by a ''photocleavage assay.'' Each pair of images shows a T7 DNA molecule before (*left*) and after (*right*) the photocleavage. DNA molecules snap back to the anchor points when they are photocleaved by exposure to illumination. Scale bars = 2.5μm. The error bar displayed is the standard error of the mean. Reprinted with permission from *Langmuir* **23**, 755 (2007). Copyright 2007 by American Chemical Society. (**C**) Fluorescently labeled RNA transcripts (*red*) formed along YOYO-stained T7 DNA (green). Scale bar = 2.5 μm

six-base-pair-long cognate sequence ''GAATTC'' which occurs at five locations on λ-DNA, yielding six fragments of different lengths. Although the DNA is bound to the surface by combing, nevertheless, all five specific locations were recognized by *Eco*RI as shown in Fig. 15. The observed cleavage sites are in good agreement with the predicted cleavage sites, which confirms that DNA molecules are cleaved by *Eco*RI rather than by photocleavage. *Eco*RI-conjugated nanoparticles can also be incubated with fluorescently labeled lambda phage DNA molecules and then stretched onto a hydrophobic surface by combing. Several examples of *Eco*RI-conjugated nanoparticles attached to DNA molecules at the expected restriction sites (Mg^{2+} was not added in order to prevent DNA cleavage), are shown to within optical resolution (Fig. 15F). We note that similar cleavage of combed DNA by *Eco*RI has been observed by Yokota et al. [58].

Other methods of stretching and immobilization of DNA molecules using moving interface include spin-coating and air-blowing [57]. Both methods rely on fast motion of an air–solvent interface, generated by the centrifugal force exerted on a droplet of DNA solution deposited on the rotating disk for spin-coating and by blowing an air jet at the side of a droplet of DNA solution placed on a hydrophobic substrate for air-blowing. The fluid flow in these methods however, is difficult to characterize and deforms the droplet of DNA solution randomly, complicating the stretching mechanism.

DNA stretching and immobilization in a micro/nano-channel

Instruments and techniques used for DNA stretching and immobilization such as optical and magnetic traps, as well as electric fields, results in small numbers of immobilized DNA molecules. In applications such as haplotyping for personalized medicine and pathogen detection by comparative genomics, analyses need to be performed on large number of stretched DNA molecules to eliminate the false positives that may arise when a fluorescent marker is attached to a non-specific sequence on the DNA molecule [59, 60]. For these purposes, there is a growing need for technology that will allow high throughput and low cost analysis of stretched and immobilized DNA molecules. A new technique that we call ''protein-assisted DNA immobilization'' (PADI) generates hundreds or thousands of stretched and immobilized DNA molecules in a microchannel [19]. The PADI technique is based on the general phenomenon of protein adsorption to hydrophobic surfaces, combined with the fact that specialized proteins that interact with DNA (such as restriction enzymes, RNA polymerases, etc.) also bind to DNA molecules. In the PADI method, DNA-interacting proteins are allowed to bind to the DNA molecule in bulk. When this DNA–protein complex is introduced into a microchannel, the DNA is stretched by hydrodynamic flow followed by DNA immobilization at the surfaces. The DNA is attached to the hydrophobic microchannel surfaces through protein adsorption, resulting in immobilization of DNA molecules inside the microchannel. Shown in Fig. 16A is an image of large number of λ-DNA molecules stretched and immobilized in a 100 μm wide and 1μm deep microchannel using RNAP as the DNA-interacting protein.

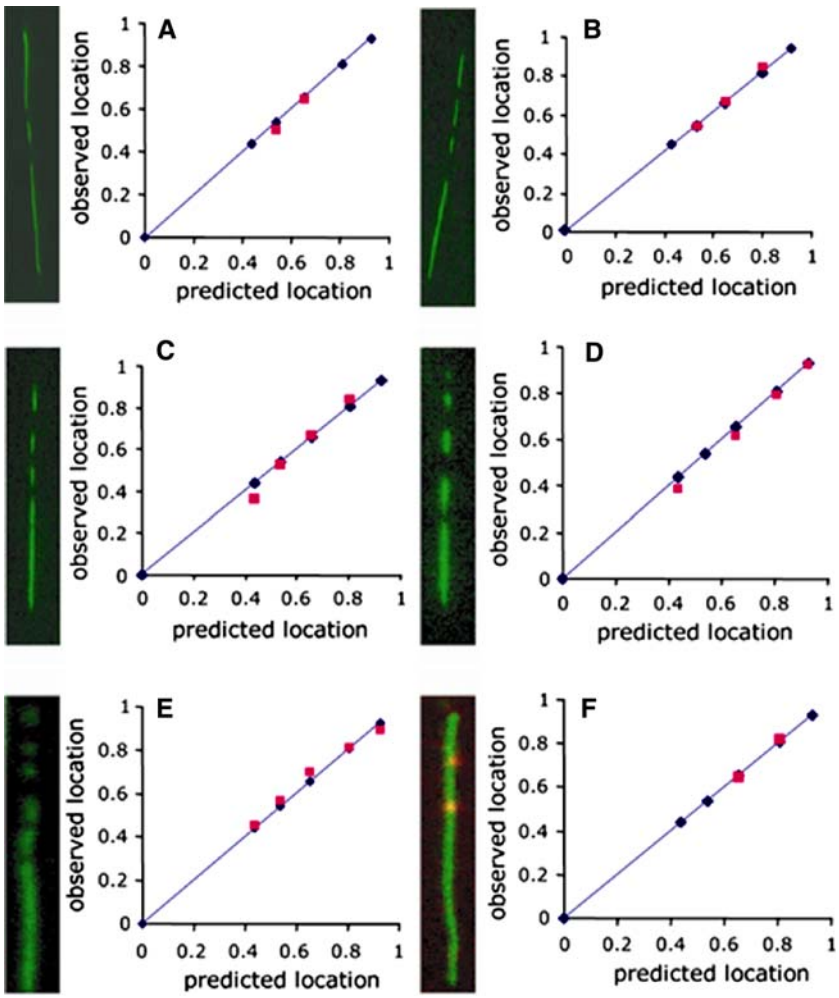

Fig. 15 (**A**)–(**E**) λ-DNA cleaved by *Eco*RI at specific locations. (**F**) *Eco*RI-conjugated fluorescent nanoparticles (red) attached to a single λ-DNA molecule. The blue diamonds are the expected restriction sites, while red squares indicate actual digestion or binding sites

The PADI technique offers several advantages over some other methods: (1) overstretching of DNA molecules is avoided; (2) the degree of attachment of DNA to the substrate can be controlled by changing the protein concentration without changing the substrate material; (3) the number of DNA molecules immobilized onto the substrate is time and concentration dependent and can be controlled simply by varying the pumping time as well as the concentration; (4) the stretching and immobilization is achieved at physiological pH; (5) inexpensive microfabricated devices are used; and (6) it only requires a couple of microlitters of sample. The ability of the PADI technique to produce different degrees of DNA attachment is demonstrated in Fig. 16B and C. At high-protein concentration, the DNA is firmly attached to the surface (Fig. 16B), while lowering the protein concentration leads to fewer proteins bound to DNA, resulting in a looser attachment of DNA to the surface (Fig. 16C).

A number of DNA–protein interactions can be performed on DNA molecules immobilized by PADI including optical mapping and transcription. We have demonstrated optical mapping of DNA molecules by first immobilizing DNA by PADI in the presence of RNAP, and then introducing type II restriction enzyme *Sma*I that cleaves DNA at ''CCCGGG'' sequence. The cleaved fragments are well preserved on the channel surface as shown in Fig. 17A. We have also demonstrated transcription of DNA molecules immobilized by PADI, similar to the experiments discussed in section ''Stretching by a moving interface''. We have stretched and immobilized T7 DNA molecules in the presence of T7 RNAP followed by introduction of transcription buffer containing NTPs and fresh RNAP. As shown in Fig. 17B, the transcripts are detected when fluorescently labeled UTPs are incorporated into the growing RNA chain, similar to those seen in the experiments of Gueroui et al. [4], discussed above.

Austin and coworkers [61] investigated the statics and dynamics of DNA molecules confined in varying size of nanochannels of various widths. The elongation of a confined polymer in the ''de Gennes regime,'' in which the channel width D is much larger than the persistence length of the DNA ($D \gg p$), is purely due to excluded volume interactions between segments of freely coiled polymer, and is predicted to scale with D as $x \cong L\left(\frac{dp}{D^2}\right)^{1/3}$, where d is

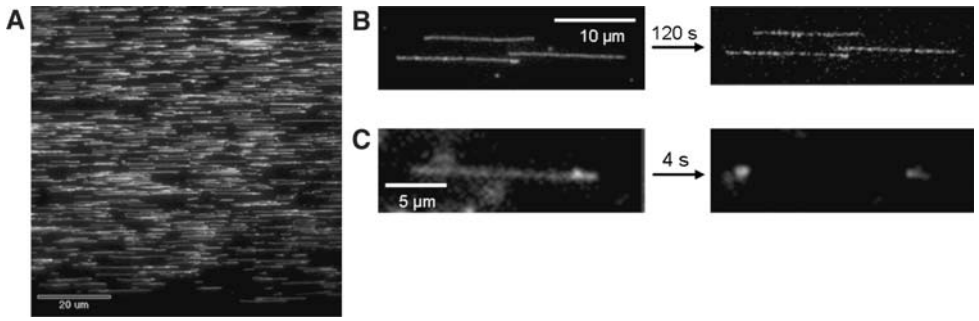

Fig. 16 (**A**) λ-DNA (5.5 pM) stretched and immobilized in the presence of T7 RNAP (10 nM). T7 DNA molecules are immobilized at (**B**) 5 nM and (**C**) 0.5 nM T7 RNAP concentration, followed by DNA photo-cleavage by exposure to illumination, revealing the number of anchor points at each concentration. All figures reprinted with permission from *Nano Lett*. **6**, 2499 (2006). Copyright 2006 American Chemical Society

the DNA diameter and L is contour length of the DNA. The extension of a confined polymer in the Odijk regime ($D \ll p$) is dominated by the interplay of confinement and intrinsic DNA elasticity. The interactions of the polymer with the channel walls extend the molecule since coiling tightly enough to fit into the channel is made energetically unfavorable. In this regime, the extension scales with D as $x \cong L[1 - 0.361(D/p)^{2/3}]$. The physics underlying the behavior of the confined polymer is not well understood at the crossover between the de Gennes and Odijk regimes. Since the channel dimension of a typical nanodevice lies near the crossover between the de Gennes and Odijk regimes (D ~ p, where p ~ 50 nm), it is therefore critical to understand the crossover behavior between two regimes. Austin and coworkers obtained the DNA extension as a function of the channel dimension by collecting the fluorescence intensity transverse to the channel axis (Fig. 18A). The deviation from the de Gennes power-law seen for the DNA in the thinnest 30 nm wide channel indicates that this channel width corresponds to the Odijk regime. By matching the expression for the DNA extension in the Odijk regime to the power-law fit, the crossover scale of $D_{\text{critical}} \sim 2\,p$ is obtained.

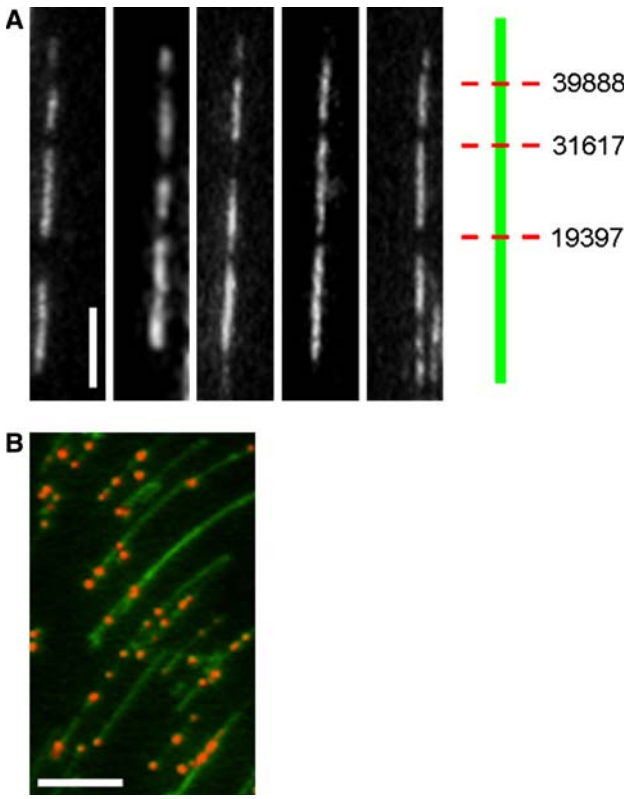

Fig. 17 (**A**) λ-DNA molecules were stretched and immobilized with T7 RNAP followed by enzymatic cleavage by *Sma*I. The location of predicted cleavage sites for *Sma*I on λ-DNA is shown on the right. Scale bar = 2.5μm. (**B**) Fluorescently labeled RNA transcripts (*red spots*) formed along YOYO-stained T7 DNA (*green lines*) immobilized by PADI. Scale bar = 5μm. All figures reprinted with permission from *Nano Lett*. **6**, 2499 (2006). Copyright 2006 American Chemical Society

Overview and final observations

We have reviewed different methods of stretching and immobilizing DNA molecules for studying single-molecule DNA–protein interactions. Single-molecule experiments overcome the problem of ensemble-averaging of molecular properties intrinsic to conventional bulk experiments by directly interrogating each molecule one at a time. Although advantageous for many purposes, single-molecule experiments also suffer the drawback that many repetitions of often-difficult and tedious experiments are required in order to obtain sufficient statistics to provide meaningful quantitative results and to determine the range of behavior possible. It is therefore critical to develop robust methods of DNA stretching and immobilization that offer both high sensitivity and high-throughput detection of DNA–protein interactions. Optical and magnetic traps allow the most accurate measurements of changes in physical properties of DNA in

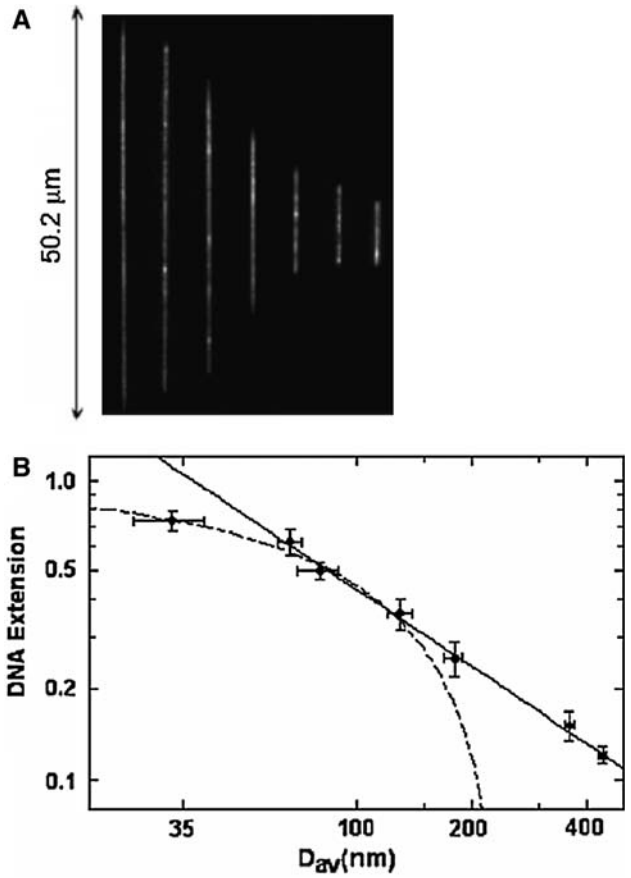

Fig. 18 (**A**) Images of T2 DNA molecules in 30 × 40 nm, 60 × 80 nm, 80 × 80 nm, 140 × 130 nm, 230 × 150 nm, 300 × 440 nm, and 440 × 440 nm channels (width × depth, left to right). (**B**) Log–log plot of normalized extension of λ-DNA as a function of the geometric average of the channel width and depth. The bold line is a power-law fit to the data for the 440, 300, 230, 140, 80, and 60 nm wide channels. The best fit exponent is –0.85 ± 0.05 which differs somewhat from the de Gennes prediction of –2/3. The dashed line is the Odjik prediction for the three smallest channels with a fitted value of $p = 52 \pm 5$ nm in agreement with the stained DNA persistence length of 57.5 ± 2 nm. All figures reprinted with permission from Reisner et al. *Phys. Rev. Lett.* **94**, 196101 (2005). Copyright 2005 by the American Physical Society

response to external force fields and physiochemical modifications by proteins. Advancements and modifications are being made to incorporate more features into these tools, such as fluorescence resonance energy transfer (FRET) that has been recently combined with the use of optical traps [62]. However, optical and magnetic traps generally are low-throughput methods, interrogating only one molecule at a time. Electrostretching could become a convenient and powerful method of stretching stretch and immobilizing multiple DNA molecules in a single run. However, more research is needed to attain more reproducible and controllable stretching by this method and to more fully understand the underlying physics.

Flow fields offer multiple alternative possibilities to stretch and immobilize DNA molecules and to study DNA–protein interactions, although a careful characterization of flow fields is required to differentiate intrinsic properties of DNA–protein interaction from the external influence. Combing of DNA molecules is perhaps the simplest form of stretching and immobilization available. This method brings DNA into close contact with the surface onto which it is immobilized, limiting its use so far to optical mapping, transcription, and fluorescence in situ hybridization [63]. Nevertheless, recent advances in combing techniques such as generating a pattern of DNA bundles [64] and stretching between lithographically patterned lines of hydrophobic polymer [65] may open new ways to use combed DNA molecules. The PADI (protein-assisted DNA immobilization) technique utilizes specific and non-specific interaction between DNA and DNA-binding proteins to stretch and immobilize DNA molecules inside a microfabricated device. Using this technique, we have been able to stretch and immobilize single ssDNA molecules in the presence of ssDNA-binding proteins. There are only a limited number of researchers that have visualized surface aligned ssDNA molecules under AFM, and none, to our knowledge, have detected with fluorescence microscopy an array of long stretched ssDNA molecules. We expect that ssDNA or RNA molecules stretched by PADI technique will bring new opportunities to study DNA hybridization, replication, RNA splicing, and post-transcriptional modifications.

References

1. H. Kabata, O. Kurosawa, I. Arai, M. Washizu, S.A. Margarson, R.E. Glass, N. Shimamoto, Science **262**, 1561 (1993)
2. Y. Harada, T. Funatsu, K. Murakami, Y. Nonoyama, A. Ishihama, T. Yanagida, Biophys. J. **76**, 709 (1999)
3. E.C. Greene, K. Mizuuchi, Mol. Cell **9**, 1079 (2002)
4. Z. Gueroui, C. Place, E. Freyssingeas, B. Berge, Proc. Natl. Acad. Sci. USA **99**, 6005 (2002)
5. J.O. Tagenfeldt, C. Printz, H. Cao, S. Chou, W.W. Reisner, R. Riehn, Y.M. Wang, E.C. Cox, J.C. Sturm, P. Silberzan, R.H. Austin, Proc. Natl. Acad. Sci. USA **101**, 10979 (2004)
6. W.-X. Shi, R. G. Larson, Nano Lett. **5**, 2476 (2005)
7. M. Guthold, X. Zhu, C. Rivetti, G. Yang, N.H. Thomson, S. Kasas, H.G. Hansma, B. Smith, P.K. Hansma, C. Bustamante, Biophys. J. **77**, 2284 (1999)
8. B.D. Sattin, M.C. Goh, Biophys. J. **87**, 3430 (2004)
9. T. Funatsu, Y. Harada, M. Tokunaga, K. Saito, T. Yanagida, Nature **374**, 555 (1995)
10. H.P. Lu, L. Xun, X.S. Xie, Science **282**, 1877 (1998)
11. Y. Harada, O. Ohara, A. Takatsuki, H. Itoh, N. Shimamoto, K. Kinosita, Jr., Nature **409**, 113 (2001)
12. A. Revyakin, R.H. Ebright, T.R. Strick, Proc. Natl. Acad. Sci. USA **101**, 4776 (2004)
13. J.F. Marko, E.D. Siggia, Macromolecules **28**, 8759 (1995)
14. A.M. van Oijen, P.C. Blainey, D.J. Crampton, C.C. Richardson, T. Ellenberger, X.S. Xie, Science **301**, 1235 (2003)

15. M. Washizu, O. Kurosawa, IEEE Trans. Ind. Appl. **26**, 1165 (1990)
16. A. Bensimon, A. Simon, A. Chiffaudel, V. Croquette, F. Heslot, D. Bensimon, Science **265**, 2096 (1994)
17. X. Michalet, R. Ekong, F. Fougerousse, S. Rousseaux, C. Schurra, N. Hornigold, M. van Slegtenhorst, J. Wolfe, S. Povey, J.S. Beckmann, A. Bensimon, Science **277**, 1518 (1997)
18. P.S. Doyle, B. Ladoux, J.-L. Viovy, Phys. Rev. Lett. **84**, 4769 (2000)
19. V.R. Dukkipati, J.H. Kim, S.W. Pang, R.G. Larson, Nano Lett. **6**, 2499 (2006)
20. A. Ashkin, J.M. Dziedzic, J.E. Bjorkholm, S. Chu, Opt. Lett. **11**, 288 (1986)
21. T.T. Perkins, D.E. Smith, R.G. Larson, S. Chu, Science **268**, 83 (1995)
22. R.G. Larson, T.T. Perkins, D.E. Smith, S. Chu, Phys. Rev. E **55**, 1764 (1997)
23. S.B. Smith, Y. Cui, C. Bustamante, Science **271**, 795 (1996)
24. H. Yin, M.D. Wang, K. Svoboda, R. Landick, S.M. Block, J. Gelles, Science **270**, 1653 (1995)
25. R.J. Davenport, G.J.L. Wuite, R. Landick, C. Bustamante, Science **287**, 2497 (2000)
26. N.R. Forde, D. Izhaky, G.R. Woodcock, G.J.L. Wuite, C. Bustamante, Proc. Natl. Acad. Sci. USA **99**, 11682 (2002)
27. B. van den Broek, M.C. Noom, G.J.L. Wuite, Nucleic. Acids Res. **32**, 3040 (2005)
28. G.M. Skinner, C.G. Baumann, D.M. Quinn, J.E. Molloy, J.G. Hoggett, J. Biol. Chem. **279**, 3239 (2004)
29. C. Gosse, V. Croquette, Biophys. J. **82**, 3314 (2002)
30. S.B. Smith, L. Finzi, C. Bustamante, Science **258**, 1122 (1992)
31. J.F. Marko, Europhys. Lett. **38**, 183 (1997)
32. B. Maier, D. Bensimon, V. Croquette, Proc. Natl. Acad. Sci. USA **97**, 12002 (2000)
33. G.J.L. Wuite, S.B. Smith, M. Young, D. Keller, C. Bustamante, Nature **404**, 103 (2000)
34. T.R. Strick, V. Croquette, D. Bensimon, Nature **404**, 901 (2000)
35. A. Ramos, H. Morgan, N.G. Green, A. Castellanos, J. Phys. D: Appl. Phys. **31**, 2338 (1998)
36. A.E. Cohen, Phys. Rev. Lett. **91**, 235506 (2003)
37. C. Walti, P. Tosch, A.G. Davies, W.A. Germishuizen, C.F. Kaminski, Appl. Phys. Lett. **88**, 153901 (2006)
38. M. Washizu, Y. Kimura, T. Kobayashi, O. Kurosawa, S. Matsumoto, T. Mamine, AIP Conf. Proc. **725**, 67 (2004)
39. V. Namasivayam, R.G. Larson, D.T. Burke, M.A. Burns, Anal. Chem. **74**, 3378 (2002)
40. M. Ueda, K. Yoshikawa, M. Doi, Polym. J. **29**, 1040 (1997)
41. R. Holzel, F.F. Bier, IEE Proc. Nanobiotechnol. **150**, 47 (2003)
42. K.E. Sung, M.A. Burns, Anal. Chem. **78**, 2939 (2006)
43. L. Zheng, J.P. Brody, P.J. Burke, Biosens. Bioelectron. **20**, 606 (2004)
44. W.A. Germishuizen, P. Tosch, A.P.J. Middelberg, C. Walti, A.G. Davies, R. Wirtz, M. Pepper, J. Appl. Phys. **97**, 014702 (2005)
45. V.R. Dukkipati, S. W. Pang, Appl. Phys. Lett. **90**, 083901 (2007)
46. H. Kabata, W. Okada, M. Washizu, Jpn. J. Appl. Phys. **39**, 7164 (2000)
47. K. Keren, R.S. Berman, E. Buchstab, U. Sivan, E. Braun, Science **302**, 1380 (2003)
48. T. Ha, X. Zhuang, H.D. Kim, J.W. Orr, J.R. Williamson, S. Chu, Proc. Natl. Acad. Sci. USA **96**, 9077 (1999)
49. T. Ha, I. Rasnik, W. Cheng, H.P. Babcock, G. Gauss, T.M. Lohman, S. Chu, Nature **419**, 638 (2002)
50. S.C. Blanchard, H.D. Kim, R.L. Gonzalez, Jr., J.D. Puglisi, S. Chu, Proc. Natl. Acad. Sci. USA **101**, 12893 (2004)
51. P.C. Blainey, A.M. van Oijen, A. Banerjee, G.L. Verdine, X.S. Xie, Proc. Natl. Acad. Sci. USA **103**, 5752 (2006)
52. P.H. von Hippel, O.G. Berg, J. Biol. Chem. **264**, 675 (1989)
53. N. Shimamoto, J. Biol. Chem. **274**, 15293 (1999)
54. J. Jing, J. Reed, J. Huang, X. Hu, V. Clarke, J. Edington, D. Housman, T.S. Anantharaman, E.J. Huff, B. Mishra, B. Porter, A. Shenker, E. Wolfson, C. Hiort, R. Kantor, C. Aston, D.C. Schwartz, Proc. Natl. Acad. Sci. USA **95**, 8046 (1998)
55. M. Chopra, L. Li, H. Hu, M.A. Burns, R.G. Larson, J. Rheol. **47**, 1111 (2003)
56. R.D. Deegan, O. Bakajin, T.F. Dupont, G. Huber, S.R. Nagel, T.A. Witten, Nature **389**, 827 (1997)
57. J.H. Kim, W.-X. Shi, R.G. Larson, Langmuir **23**, 755 (2007)
58. H. Yokota, F. Johnson, H. Lu, R.M. Robinson, A.M. Belu, M.D. Garrison, B.D. Ratner, B.J. Trask, D.L. Miller, Nucleic. Acids Res. **25**, 1064 (1997)
59. P.Y. Kwok, M. Xiao, Hum. Mutat. **23**, 442 (2004)
60. T. Slezak, T. Kuczmarski, L. Ott, C. Torres, D. Medeiros, J. Smith, B. Truitt, N. Mulakken, M. Lam, E. Vitalis, A. Zelma, C.E. Zhou, S. Gardner, Brief. Bioinform. **4**, 133 (2003)
61. W. Reisner, K.J. Morton, R. Riehn, Y.M. Wang, Z. Yu, M. Rosen, J.C. Sturm, S.Y. Chou, E. Frey, R.H. Austin, Phys. Rev. Lett. **94**, 196101 (2005)
62. R.R. Brau, P.B. Tarsa, J.M. Ferrer, P. Lee, M.J. Lang, Biophys. J. **91**, 1069 (2006)
63. P. Philippe, A. Bensimon, E. Schwob, Genes Dev. **16**, 2479 (2002)
64. J. Guan, L.J. Lee, Proc. Natl. Acad. Sci. USA **102**, 18321 (2005)
65. D.C.G. Klein, L. Gurevich, J.W. Janssen, L.P. Kouwenhoven, J.D. Carbeck, L.L. Sohn, Appl. Phys. Lett. **78**, 2396 (2001)